AN EULER AERODYNAMIC METHOD FOR LEADING-EDGE VORTEX FLOW SIMULATION

Pradeep Raj
Lockheed - California Company
Burbank, California

Lyle N. Long
Lockheed - Advanced Aeronautics Company
Valencia, California

SUMMARY

This paper describes the current capabilities and the future plans for a three-dimensional Euler Aerodynamic Method. The basic solution algorithm is based on the finite-volume, Runge-Kutta pseudo-time-stepping scheme of FLO-57. Several modifications to improve accuracy and computational efficiency have been incorporated and others are being investigated. The computer code is used to analyze a cropped delta wing at 0.6 Mach number and an arrow wing at 0.85 Mach number. Computed aerodynamic parameters are compared with experimental data. In all cases, the configuration is impulsively started and no Kutta condition is applied at sharp edges. The results indicate that with additional development and validation, the present method will be a useful tool for engineering analysis of high-speed aircraft.

INTRODUCTION

The simulation of three-dimensional vortices interacting with lifting surfaces is of considerable importance to aircraft designers. This problem is of special significance for supersonic-cruise aircraft which have highly swept slender wings. At moderate-to-high angles of attack, the flow invariably separates from the leading edges resulting in the formation of free vortices above the wing. Significant improvements in aerodynamic performance can be derived, as shown in Figure 1, by careful generation and control of these vortices. At the present time, a designer has to rely on extensive and costly wind-tunnel tests. The development of accurate, efficient, and reliable computational methods will provide a more economical means of designing aerospace vehicles.

Past research on leading-edge-separated-flow simulation has produced a variety of computational methods. At one end of the spectrum are the vortex-lattice (Refs. 1-4) and free-vortex-sheet methods (Refs. 5,6). Since they are based on a linearized potential-flow formulation, rotational vortex flow cannot be predicted as part of the solution. The leading-edge vortex has to be explicitly modeled either indirectly using the suction analogy of Polhamus (Ref. 7) or directly using singularity distributions (Refs. 4,5). At the other end of the spectrum are the finite-difference methods based on the Reynolds-averaged Navier-Stokes equations (Ref. 8) which provide an essentially complete fluid-dynamic model. Their use offers the major advantage that the leading-edge vortices result as a part of the solution. However, the available methods are not suitable for routine practical applications due to the exorbitant requirements of computational resources and the lack of a suitable universal turbulence model.

Recent advances in numerical algorithms to solve the Euler equations (Refs. 9,10) provide an attractive and cost-effective alternative to using Navier-Stokes codes. Their ability to automatically capture regions of rotational flows has been demonstrated by several investigations (Refs. 11-15). In this paper, the current

status and planned development of a three-dimensional Euler Aerodynamic Method (TEAM) and its application to model leading-edge separated flow about a cropped-delta wing and an arrow wing are presented.

TEAM represents a modular computational system being developed by the Lockheed-California Company for analyzing complete aircraft configurations. A schematic of the system is shown in Figure 2. This development is being partially funded by the U. S. Air Force Wright Aeronautical Laboratory (AFWAL)/Flight Dynamics Laboratory (FDL) under a three-year contract (F33615-84-C-3005). The basic features of the method are described in the next section.

THREE-DIMENSIONAL EULER AERODYNAMIC METHOD

The explicit pseudo-time-stepping, finite-volume algorithm of Jameson et al. (Ref. 9), modified by Lockheed-California Company over the past three years, forms the core of the TEAM code. Jameson's original wing-alone code is widely known as FLO-57. The region surrounding a given configuration is subdivided into small cells. In each of the cells, the time-dependent Euler equations (in integral equation form), representing the mass, momentum, and energy conservation, are integrated in time using a multi-stage Runge-Kutta scheme. To accelerate convergence to the steady state, local rather than global time steps are used. Implicit residual smoothing (Ref. 16) further reduces the number of time steps required to reach the steady state. Appropriate non-reflecting boundary conditions based on Riemann invariants (Ref. 16) are used at the far-field boundaries and no-normal-flow conditions are used on the solid surface.

The finite-volume formulation essentially decouples the flow solver from the grid generator. The grids can be constructed in any convenient manner; only the Cartesian coordinates of the nodal points are required by the solver. This aspect of the basic algorithm has been exploited to build the TEAM system for analyzing complete aircraft configurations. An overview of the four major modules (Figure 2) constituting the system is presented in this section.

TEAM PREPROCESSOR MODULE

This module will provide a capability to process geometry-definition data supplied by a designer in order to construct an accurate geometrical model of a configuration and a suitable grid on its surface. The designer-supplied data typically contain a series of cross-sectional curves defining various components. In some instances, the configuration may be geometrically defined for some other aerodynamic analysis code. Constructing a model that accurately reflects the information contained in this form is the crucial first step. A surface grid on this model forms the key input for any grid-generation method. Appropriate interfaces are being developed to accomplish these tasks using the Configuration Data Management System (CDMS), which Lockheed - Georgia Company is developing for the U.S. Air Force under contract F33615-84-C-3001.

TEAM GRID GENERATOR MODULE

A variety of techniques, both algebraic and differential, are included in the grid-generator module, as shown in Figure 3. This is essential because, at the present time, there is no single method that can be used to generate suitable grids for all configurations. The current capabilities of the various methods are summarized in Figure 4. Their desirable features are also compared in the same figure. For instance, the algebraic Trans-Finite Interpolation (TFI) method is computationally

efficient and powerful but requires considerable user interaction to generate suitable grids as compared to the differential-equation methods, such as the Boundary Integral Grid (BIG) generation method (Ref. 17). This automation is achieved at the expense of computational efficiency. The Parabolic Conformal Mapping with Shearing (PACMAPS) technique (Ref. 18) is computationally efficient and easy to use; however, the grids must be of C-H topology. The C-H grid topology is illustrated in Figure 5.

Two diagnostic tools are crucial to the grid-generator module: Lockheed's PLOT3D program for interactively displaying grids and an analytical grid checking program. The grid checker can automatically locate regions where the grid lines either cross or are highly skewed. These regions are then further examined using PLOT3D and modified as necessary.

TEAM FLOW SOLVER MODULE

As mentioned above, the flow solver is based on the finite-volume, pseudo-time-marching algorithm of Jameson et al. (Ref. 9). Since the mathematical and numerical features of the basic scheme are adequately described in References 9 and 19, they will not be repeated here. Several modifications have been and are being incorporated by Lockheed to enhance the capabilities of the solver as summarized in Figure 6. These modifications are briefly described below.

Flux Computation. -- The cell-centered finite-volume scheme used for spatially discretizing the Euler equations expresses the time-rate of change of a flow quantity in a cell as the net flux through the surfaces of the cell. A variety of approximations can be used to numerically compute this flux. The current version of the code uses a strongly conservative formulation. It is compared with the original FLO-57 formulation in Figure 7. Quantitative improvement in accuracy is under investigation.

Numerical Dissipation. -- The present finite-volume scheme reduces to a central-difference scheme on a uniform grid. To suppress the well-known tendency for odd and even point decoupling of such schemes, and to limit the generation of wiggles and overshoots near shock waves, blended second and fourth differences have to be added. The coefficient of the second-order terms is proportional to the local pressure gradient. Therefore, these terms are turned on only where larger amounts of dissipation are needed, e.g., near shocks and stagnation points. Elsewhere, the fourth-difference terms keep the dissipation small.

The dissipation terms are approximated by central-difference formulas for all cells except those near the boundaries. In the original FLO-57 code, the contribution of η-direction terms (normal to the surface) was ignored for cells adjacent to the boundaries. This approach, designated Scheme 1 here, leads to an erroneous production of entropy. To eliminate this deficiency, alternative schemes have been incorporated.

All those cells that do not abut the solid surface (including the ones aft of the trailing edge) were treated like any other interior cell. For those adjacent to the solid boundary, four schemes are available. The order of approximation of the η-direction differences for these schemes is compared in Figure 8. An extensive evaluation is in progress in order to select one of these schemes for the solver. For the results shown in this paper, Scheme 2 is used.

Surface Boundary Conditions. -- On a solid surface, the no-normal-flow boundary condition is imposed by setting all convected flux quantities to zero. Only the pressure on the solid surface contributes to the momentum flux balance. Since

pressure is calculated at the cell center, one is forced to estimate its value at the actual surface. This is accomplished by computing the derivative of pressure normal to the surface using the momentum equation:

$$\rho \, \bar{V} \cdot (\bar{V} \cdot \nabla) \, \hat{n} = \hat{n} \cdot \nabla p$$

where: V, n, and p are the fluid velocity, surface normal, and pressure, respectively. This derivative and the cell-centered values are then combined to determine the surface pressure. A precise implementation requires that all metric quantities and flow variables occurring in the equation above be evaluated right on the surface. In the original FLO-57 program, this was not done; the cell-center values were used instead. In the present version of the solver, three additional approaches may be used to obtain the desired flow variables on the actual surface: (1) A Taylor series expansion about the cell center, (2) Lagrange two-point extrapolation along the local normal direction, and (3) Averaging the cell-center values for cells next to the surface in the flow domain and ghost cells outside of the flow domain. An extensive evaluation of the different approaches is under way.

Grid Topologies. -- The present version of the solver can accommodate single global grids of various topologies. The original FLO-57 solver was limited to isolated wings having C-H grids, whereas the O-O and C-O types offer improved resolution (Ref. 20). If a C-H mesh is used, adequate resolution near the wing tip can be obtained only by increasing the number of cells in the spanwise direction. It must be noted that none of these topologies is as suitable as the H-H when detailed flow field about all sections of a wing-body or wing-body-tail configuration is desired. With these considerations, the solver was modified to accommodate O-O, C-O and H-H grids, in addition to the C-H.

Patched Zonal Solver. -- The development of a zonal solver is motivated by the need to analyze complex geometries and to improve computational efficiency. For complex geometries, e.g., a complete aircraft, it becomes extremely difficult to generate a single global grid. The difficulty is further aggravated by the necessity to cluster cells in regions of large flow gradients. These problems can be largely alleviated by dividing the flow domain into a number of zones and by constructing the grid in each zone independently.

A significant improvement in computational efficiency may be achieved by using refined meshes in zones where large gradients in flow variables are expected and using relatively coarse meshes elsewhere. Work is presently under way to develop a solver that can accommodate patched zonal grids. The feasibility of this approach has been demonstrated for two dimensions by Rai (Ref. 21).

TEAM POSTPROCESSOR MODULE

This module is composed of sub-modules to accurately determine forces and moments using the flow variables computed by the solver and to graphically display surface pressure distributions, flow-field velocity vectors, and iso-parametric contours.

The surface-pressure integration method for computing forces and moments is currently used in the code. This method is only accurate when a relatively fine grid is used. Small errors in surface pressures and geometry can lead to large errors in drag. Also, this approach cannot give an estimate of how the total drag is split into lift-induced and wave drag. Alternative approaches are being pursued.

For graphically displaying data, appropriate interfaces will be developed for linking the TEAM code with CDMS.

RESULTS

A number of configurations have been analyzed using the TEAM code during its development to date. Results for a cropped delta wing and an arrow wing are presented here. For each case, the entire region is initialized to free-stream conditions. This is equivalent to impulsively starting the configuration. No Kutta condition is explicitly applied at the sharp edges.

CROPPED DELTA WING

This wing has a leading-edge sweep of 63 degrees, a taper ratio of 0.1, and an aspect ratio of 1.64. Its cross section is a NACA 63A002 airfoil. It was analyzed using the TEAM code at a Mach number of 0.6 and angles of attack of 8, 16, and 24 degrees. Two grids were used, one having 24,576 (96x16x16) cells and the other having 98,304 (96x32x32) cells. Both were topologically C-H. The airfoil sections are defined by 30 cells on both the upper and lower surfaces (for both grids). In the spanwise direction the wing is described by 10 cells for the coarse grid and 20 cells for the finer grid. Between the wing and the far-field, there are 16 and 32 cells for the two grids respectively. The C-curves are clustered around the wing using a control curve (Ref. 18).

The computed aerodynamic forces and moments are compared with the experimental data (Ref. 22) in Figure 9. The overall agreement between the predictions and the measurements is good. The code is able to model the nonlinear nature of the flow. The differences between the predictions can be traced to the differences in flow resolution provided by the two grids. This is illustrated by cross-plane surface pressure distributions at x/c = 0.6 and 0.9 (where c is the root chord) shown in Figure 10 and the corresponding velocity vectors in Figure 11 for the 16-degree angle-of-attack case. The presence of a leading-edge separated vortex is clearly shown in Figure 11.

One aspect of this particular configuration deserves special attention. The convergence history plot for the coarse mesh presented in Figure 12 shows that the average error (net mass-flux) is reduced by 4 orders of magnitude for all the cases. The fine mesh results also converge for the 8 and 16 degrees angle-of-attack cases, as shown in Figure 13.

However, the fine mesh results clearly do not converge at 24 degrees angle of attack. It is interesting to note that the experimental data (Figure 9) shows a definite break in the lift-curve slope above approximately 20 degrees angle of attack; and, as shown by the horizontal line in Figure 9, the predicted lift oscillates about the experimental data. In the absence of detailed experimental data on the flow field, one can only speculate on the flow phenomena involved here. The leading-edge vortex bursting and/or massive viscous separation could be responsible. The set of computed cross-plane pressure distributions and velocity-vector plots shown in Figure 14 indicate that the leading-edge vortex is essentially stable after 600 cycles at x/c=0.6 cross-plane; but, as shown in Figure 15, its structure and location are changing continuously at x/c=0.9 cross-plane. This latter fact is responsible for the lack of convergence seen in Figure 13. It would be most interesting to obtain more detailed experimental data and compare them to these numerical results in order

to validate the predictions of the code. Of course, the time histories shown here cannot be taken literally since pseudo-time marching was used and they are not time accurate.

It is quite obvious from the studies to date that a refined grid is essential to the simulation of leading-edge vortex flows even for relatively simple wings. Additional studies are needed to answer the obvious question: "How refined should a grid be?" Lockheed is conducting such studies under an on-going cooperative program with NASA Langley Research Center. Since the TEAM code is being developed to analyze entire aircraft configurations, studies such as these will help determine the number of cells required to adequately predict leading-edge vortex flows on complex configurations.

ARROW WING

The next set of results is for an arrow wing with a leading-edge sweep of 71.2 degrees, a taper ratio of 0.1, and an aspect ratio of 1.4. The wing was analyzed at 0.85 Mach number and -4, 8, and 16 degrees angle of attack using a C-H grid having 98,304 (96x32x32) cells.

The computed normal force and pitching moment coefficients are compared with experimental data (Ref. 23) in Figure 16. Cross-plane surface pressure distributions are compared to experimental data for four locations in Figure 17. Velocity vector plots for the same locations are shown in Figure 18. Measured velocity vectors are not available for this configuration. However, recent advances in Laser-Doppler Velocimetry (Ref. 24) now make it possible to compare measured and predicted velocity vectors for complicated three-dimensional flow fields.

Additional studies are under way to use even more refined grids to determine the source of discrepancy between the theory and measurements. Two possible sources are: (1) the experiments were conducted for a wing-body configuration whereas the computations are for an isolated wing, and (2) the present wing has a rounded leading edge and the point of separation may not be correctly located by the present code. These issues will be addressed in future studies.

CONCLUDING REMARKS

The current status and proposed development of a three-dimensional Euler Aerodynamic Method (TEAM) were presented in this paper. Correlations of computed aerodynamic parameters and surface pressure distributions with experimental data indicate its ability to capture leading-edge separated vortices. Unlike the procedures based on velocity potential, it is not required to explicitly model these vortices. In addition, the same code can be used for analysis throughout the subsonic, transonic, and supersonic flight regimes. The results presented in this paper point to a need for more extensive validation. A number of questions, especially related to the effect of grid density and numerical dissipation on the solution, remain to be answered. With continuing development and validation, it promises to provide an effective engineering tool for analyzing nonlinear flows containing both shock waves and leading-edge-separated vortices.

REFERENCES

1. Lamar, J. E., "Extension of Leading-Edge-Suction Analogy to Wings with Separated Flow Around the Side Edges at Subsonic Speeds," NASA TR R-428, October 1974.

2. Lamar, J. E. and Gloss, B. B., "Subsonic Aerodynamic Characteristics of Interacting Lifting Surfaces with Separated Flow Around Sharp Edges Predicted by a Vortex-Lattice Method," NASA TN D-7921, September 1975.

3. Lan, C. E. and Chang, Jen-Fu, "Calculation of Vortex Lift Effect for Cambered Wings by Suction Analogy," NASA CR 3449, July 1981.

4. Mehrotra, S. C. and Lan, C. E., "A Theoretical Investigation of the Aerodynamics of Low-Aspect-Ratio Wings with Partial Leading-Edge Separation," NASA CR 145304, 1978.

5. Johnson, F. T., Lu, P., Tinoco, E. N., and Epton, M. A., "An Improved Panel Method for the Solution of Three-dimensional Leading-edge Vortex Flows," NASA CR 3279, July 1980.

6. Luckring, J. M., Schoonover, W. E., and Frink, N. T., "Recent Advances in Applying Free Vortex Sheet Theory for the Estimation of Vortex Flow Aerodynamics," AIAA 82-0095, 20th Aerospace Sciences Meeting, Orlando, Florida, January 11-14, 1982.

7. Polhamus, E. C., "A Concept of the Vortex Lift of Sharp Edge Delta Wings Based on a Leading-Edge-Suction Analogy," NASA TN D-3767, 1966.

8. Fujii, K. and Kutler, P., "Numerical Simulation of the Leading-Edge Separation Vortex for a Wing and Strake-Wing Configuration," AIAA Paper 83-1908-CP, 6th Computational Fluid Dynamics Conference, Danvers, Massachusetts, July 13-15, 1983.

9. Jameson, A., Schmidt, W., and Turkel, E., "Numerical Solutions of the Euler Equations by Finite Volume Methods Using Runge-Kutta Time-Stepping Schemes," AIAA Paper 81-1259, 14th Fluid and Plasma Dynamics Conference, Palo Alto, California, June 23-25, 1981.

10. Rizzi, A., "Damped Euler Equation Method to Compute Transonic Flow Around Wing-Body Combinations," AIAA Journal, Vol. 20, No. 10, October 1982, pp. 1321-1328.

11. Hitzel, S. M. and Schmidt, W., "Slender Wings with Leading-Edge Vortex Separation -- A Challenge for Panel Methods and Euler Codes," AIAA Paper 83-0562, 21st Aerospace Sciences Meeting, Reno, Nevada, January 10-13, 1983.

12. Raj, P. and Sikora, J. S., "Free-Vortex Flows: Recent Encounters with an Euler Code," AIAA Paper 84-0135, 22nd Aerospace Sciences Meeting, Reno, Nevada, January 9-12, 1984.

13. Rizzi, A., "Computer Simulation of Non-potential Flows Around Wings," Aeronautical Journal, June/July 1984, pp. 238-248.

14. Raj, P., "Computational Simulation of Free-Vortex Flows Using An Euler Code," ICAS-84-1.3.1, 14th Congress of the International Council of the Aeronautical Sciences, Toulouse, France, September 9-14, 1984.

15. Rizzi, A. and Eriksson, L.E., "Computation of Flow Around Wings Based on the Euler Equations," Journal of Fluid Mechanics, Vol. 148, November 1984, pp. 45-71.

16. Jameson, A. and Baker, T. J., "Solution of the Euler Equations for Complex Configurations," AIAA Paper 83-1929-CP, 6th Computational Fluid Dynamics Conference, Danvers, Massachusetts, July 13-15, 1983.

17. Sikora, J. S. and Miranda, L. R., "Boundary Integral Grid Generation Technique," AIAA Paper 85-4088, 3rd Applied Aerodynamics Conference, Colorado Springs, Colorado, October 14-16, 1985.

18. Raj, P., "PACMAPS: A Three-dimensional Grid Generation Method, Version 1.0," LR 30811, Lockheed-California Company, October 1984.

19. Agarwal, R. K. and Deese, J. E., "Transonic Wing-Body Calculations Using Euler Equations," AIAA Paper 83-0501, 21st Aerospace Sciences Meeting, Reno, Nevada, January 10-13, 1983.

20. Eriksson, L. E., "Generation of Boundary-Conforming Grids About Wing-Body Configurations Using Transfinite Interpolation," AIAA Journal, Vol. 20, No. 10, October 1982, pp. 1313-1320.

21. Rai, M. M., "A Conservative Treatment of Zonal Boundaries for Euler Equation Calculations," AIAA Paper 84-0164, 22nd Aerospace Sciences Meeting, Reno, Nevada, January 9-12, 1984.

22. Emerson, H. F., "Wind-Tunnel Investigation of the Effect of Clipping the Tips of Triangular Wings of Different Thickness, Camber, and Aspect Ratio - Transonic Bump Method," NACA TN 3671, June 1956.

23. Manro, M. E., Manning, K. J. R., Hallstaff, T. H., and Rogers, J. T., "Transonic Pressure Measurements and Comparison of Theory to Experiment for an Arrow-Wing Configuration," NASA CR-2610, August 1976.

24. Novak, C. J., Huie, C. R., and Cornelius, K. C.; "Laser Velocimetry in Highly Three-Dimensional and Vortical Flows," Vortex Flow Aerodynamics - Volume I, NASA CP-2416, paper no. 7, 1986.

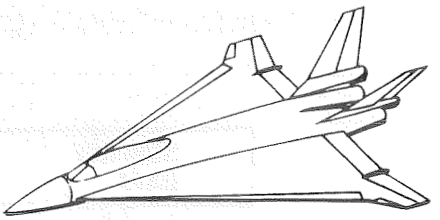

- INCREASED MANEUVER LIFT
- INCREASED LANDING AND TAKEOFF LIFT
- LIGHT WEIGHT
- AERODYNAMIC CENTER CONTROL
- LITTLE INCREASE IN GUST RESPONSE
- REDUCED BUFFET INTENSITY

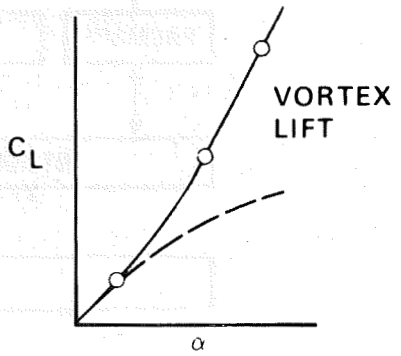

Figure 1. Benefits of vortex flow for high-speed aircraft.

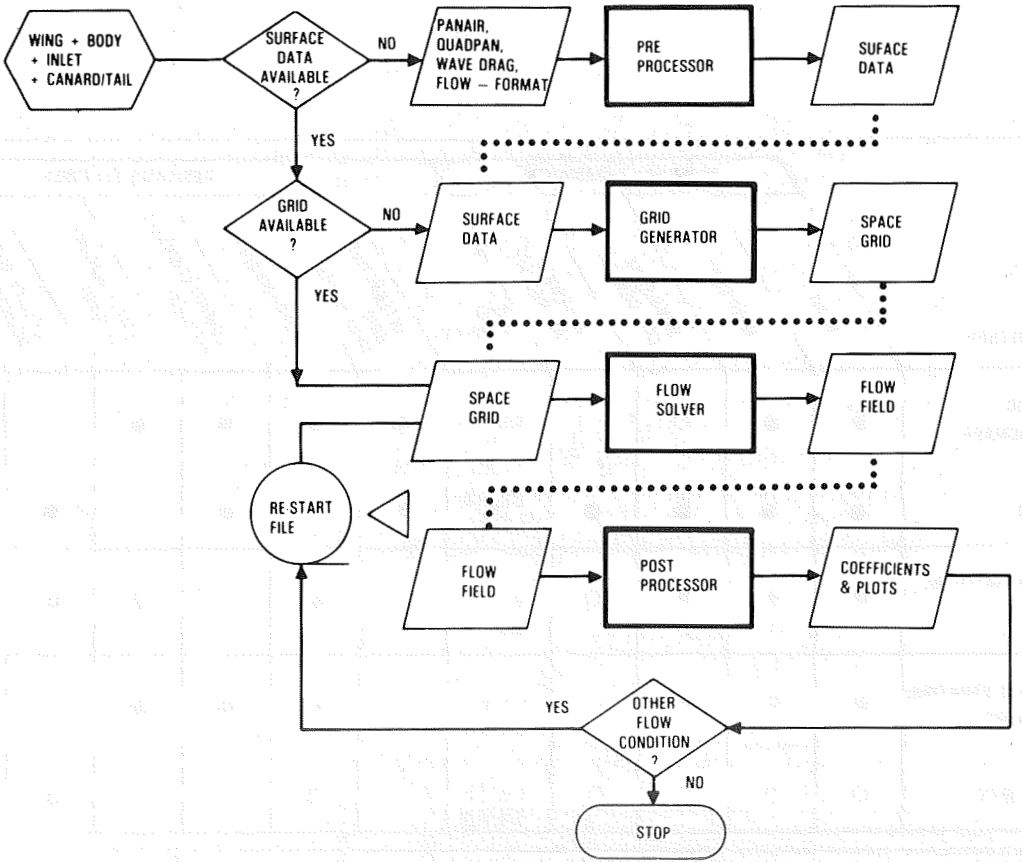

Figure 2. Lockheed-California Company's three-dimensional Euler aerodynamic method (TEAM).

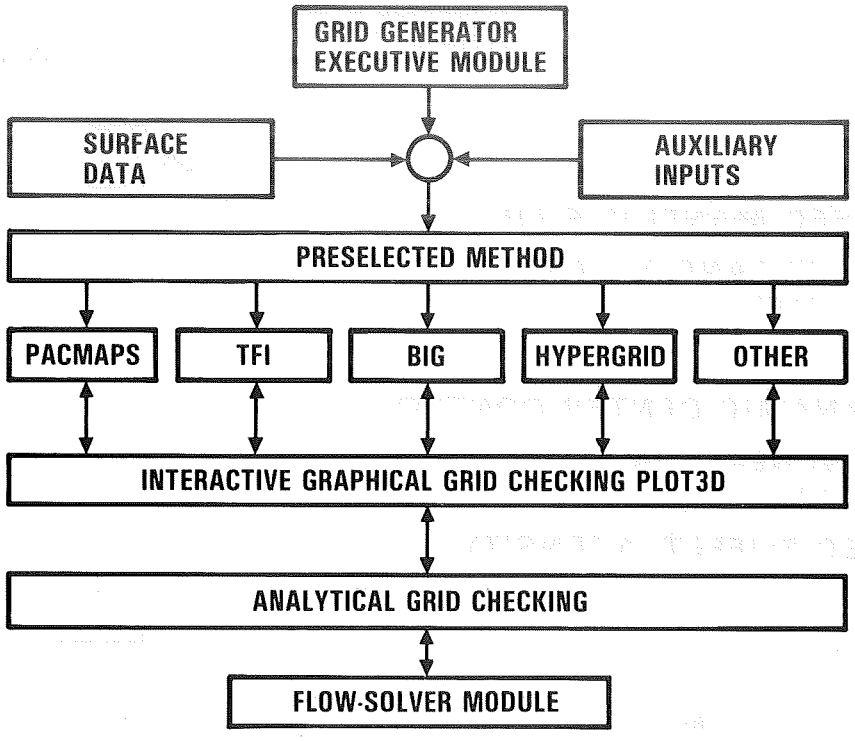

Figure 3. Schematic of TEAM's grid generator module.

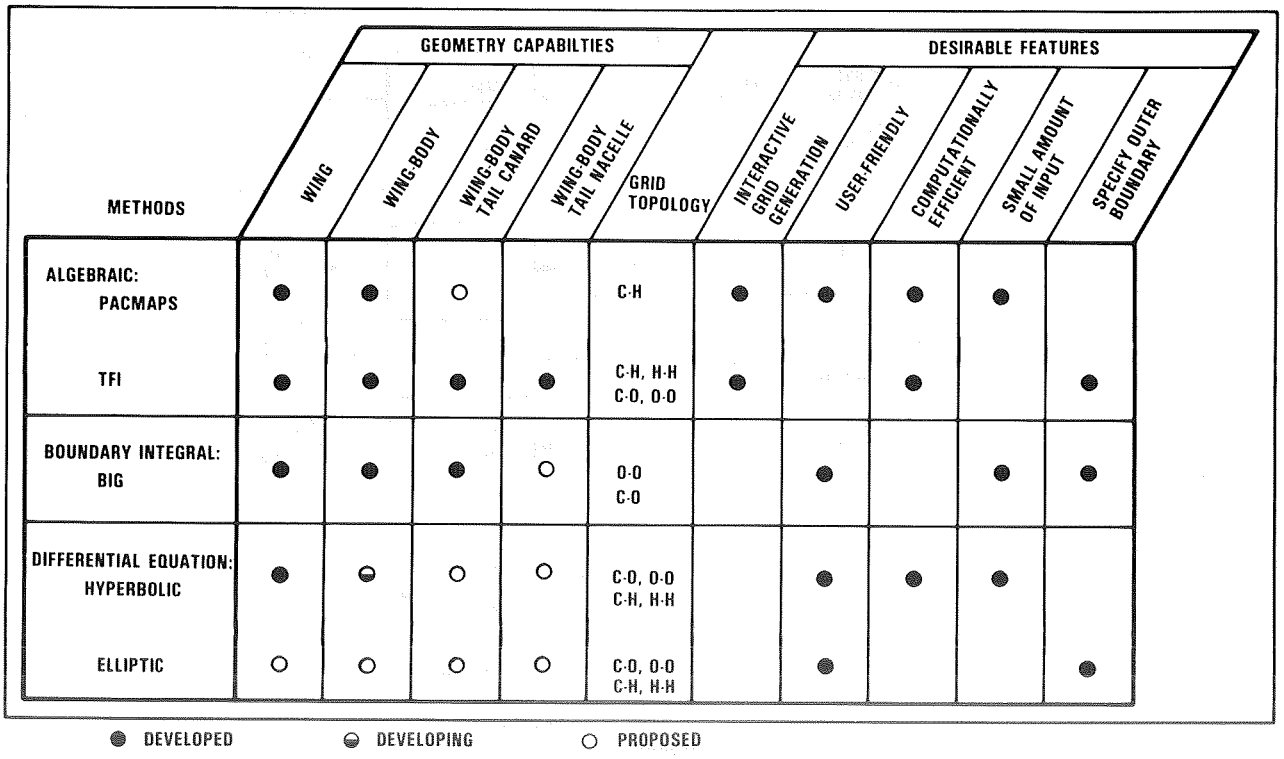

Figure 4. Lockheed-California Company's grid generation methods.

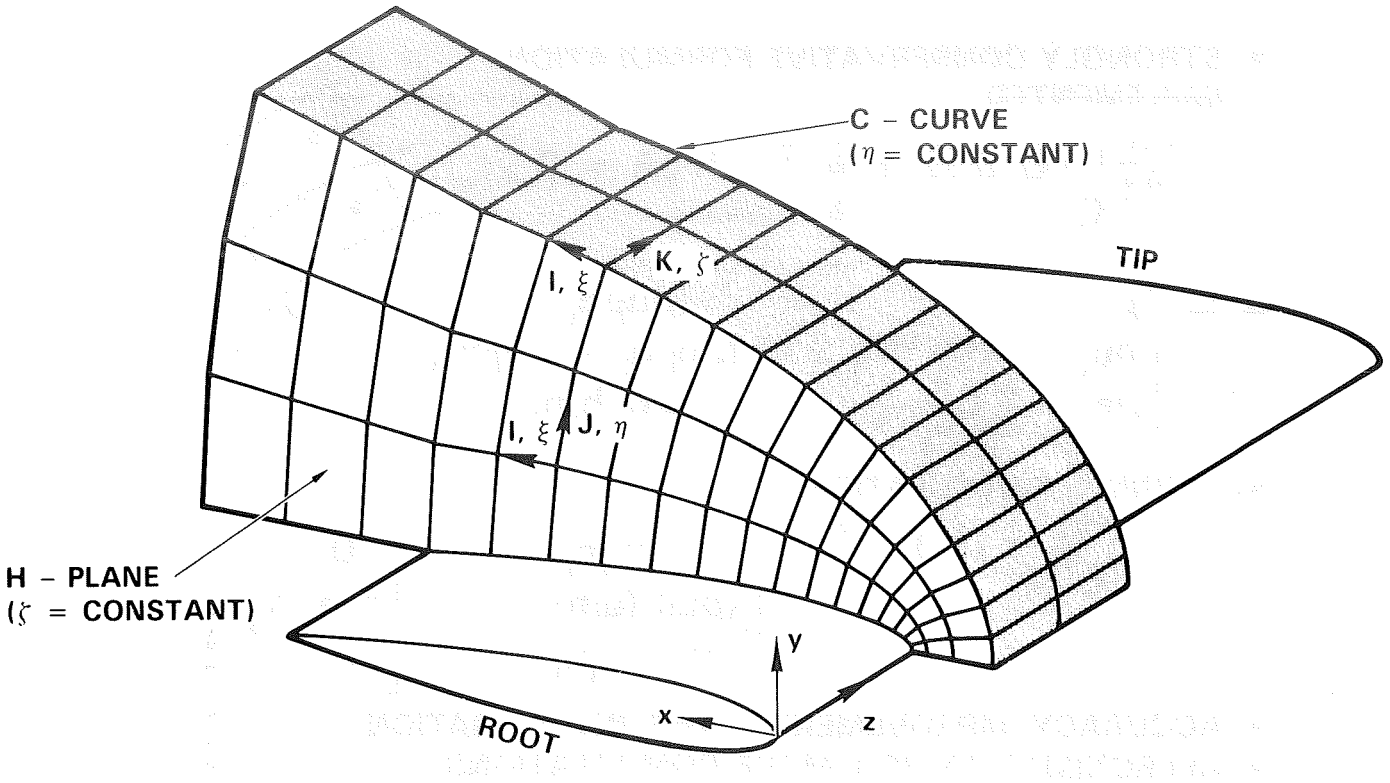

Figure 5. Example of a C-H grid.

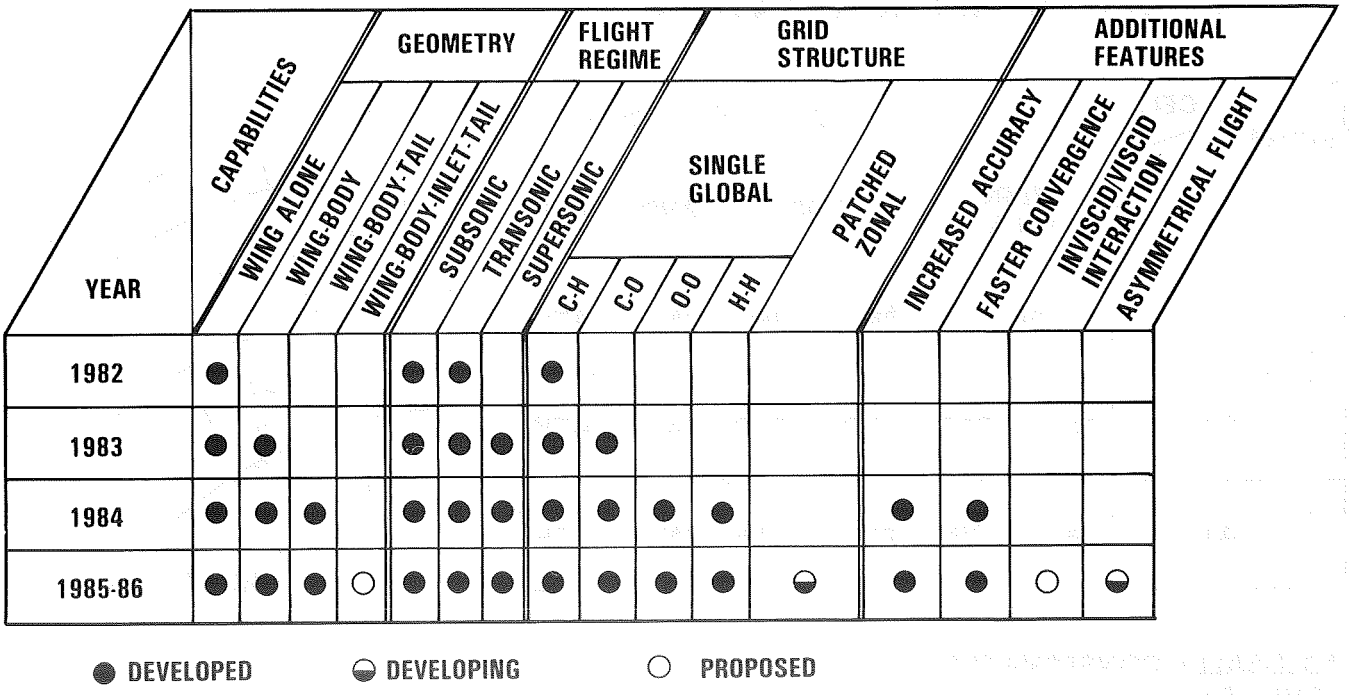

Figure 6. Capabilities of TEAM's flow solver module.

- **STRONGLY CONSERVATIVE FORMULATION IMPLEMENTED**

$$\frac{\partial}{\partial t}\iiint_{\Omega} Q \, d\Omega + \oiint_{A} \vec{F} \cdot \hat{n} \, dA = 0$$

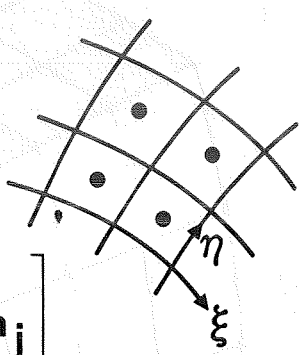

$$Q \equiv \begin{bmatrix} \rho \\ \rho u_i \\ \rho e \end{bmatrix} \qquad \vec{F} \cdot \hat{n} = \begin{bmatrix} (\rho u_i) n_i \\ (\rho u_i u_j + p\delta_{ij}) n_j \\ (\rho u_i h) n_i \end{bmatrix}$$

- **ORIGINAL FORMULATION**

$$\vec{F} \cdot \hat{n} = \begin{bmatrix} \rho\,(u_i n_i) \\ (\rho u_i)\,(u_j n_j) \\ (\rho h)\,(u_i n_i) \end{bmatrix} + \begin{bmatrix} 0 \\ p\, n_i\, \delta_{ij} \\ 0 \end{bmatrix}$$

- **ACCURACY IMPROVEMENT UNDER INVESTIGATION**
- **APPROXIMATELY 30% MORE COMPUTATIONS**

Figure 7. Comparison of TEAM and FLO-57 convective flux computation.

ORDER OF APPROXIMATION

SCHEME \ CELL	1	2	⩾ 3
1	(ZERO FLUX)	2ND	2ND + 4TH
2	2ND	2ND + 3RD	2ND + 4TH
3*	1ST + 2ND	2ND + 3RD	2ND + 4TH
4†	2ND + 3RD	2ND + 4TH	2ND + 4TH

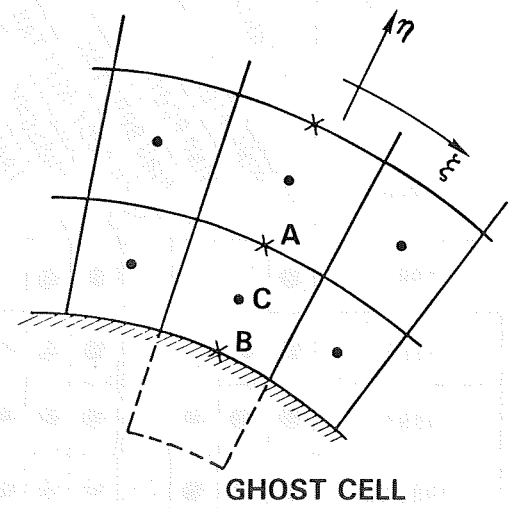

*GLOBALLY CONSERVATIVE
†GHOST CELLS

Figure 8. Four schemes for calculating dissipation terms near a solid surface.

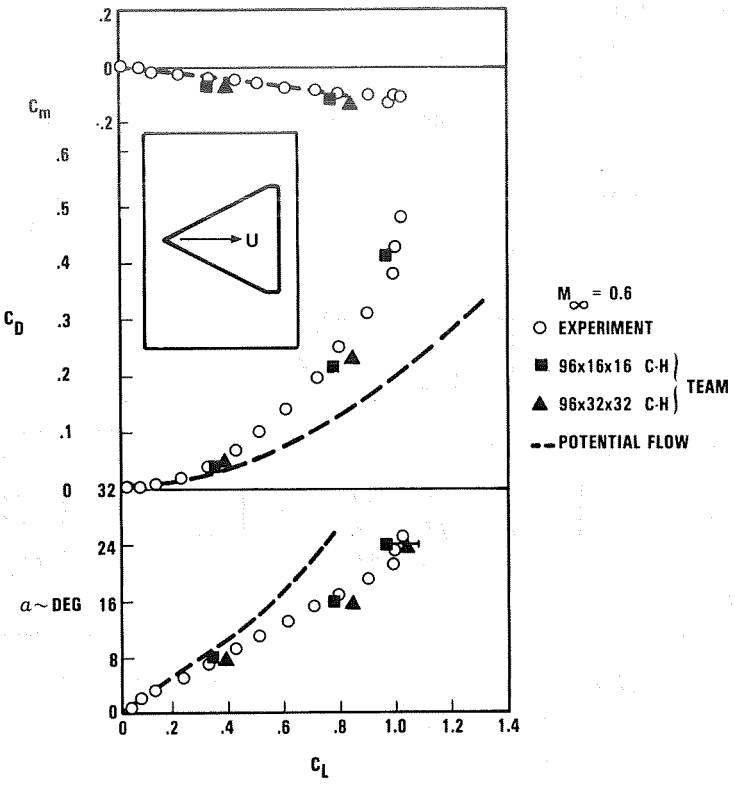

Figure 9. TEAM code results compared to experimental values for a cropped delta wing.

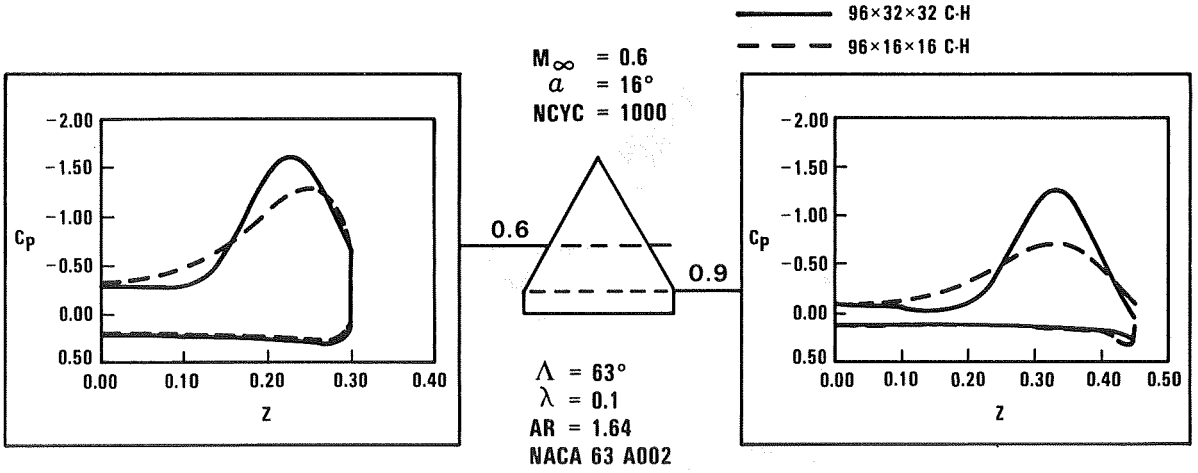

Figure 10. Predicted spanwise pressure distributions for two grids.

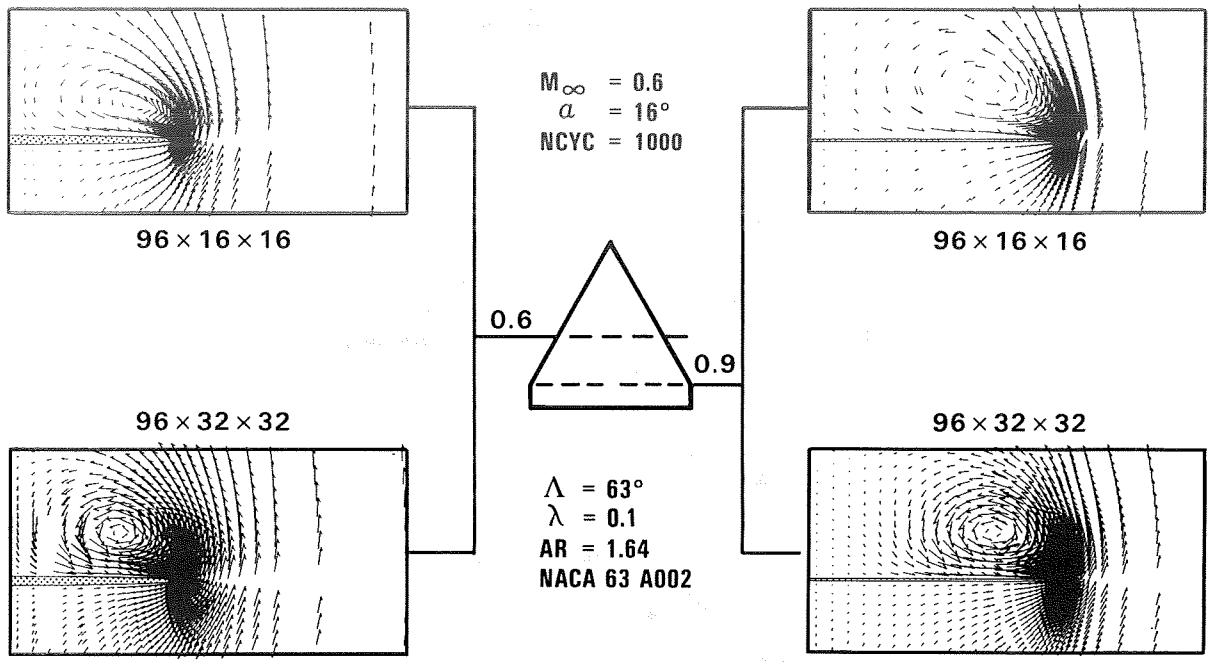

Figure 11. Cross-flow velocity vectors for two grids and two chordwise locations.

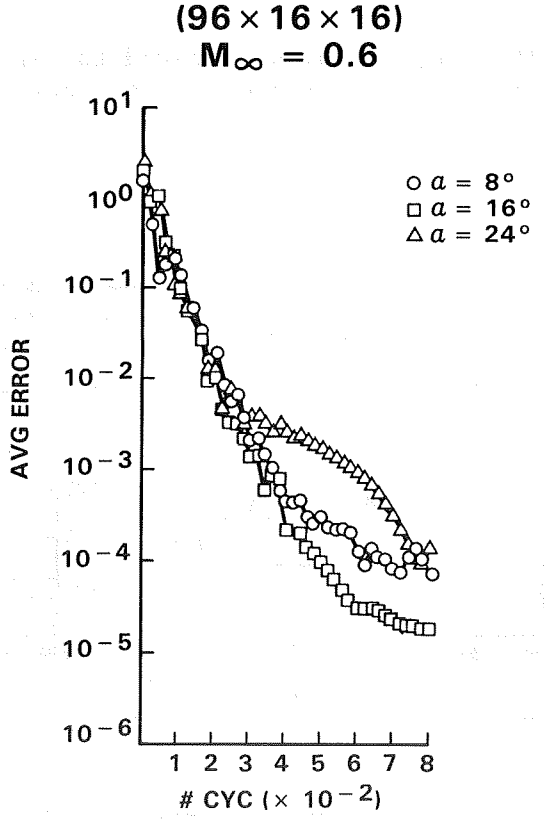

Figure 12. Convergence history for a coarse grid (96 × 16 × 16) at three different angles of attack.

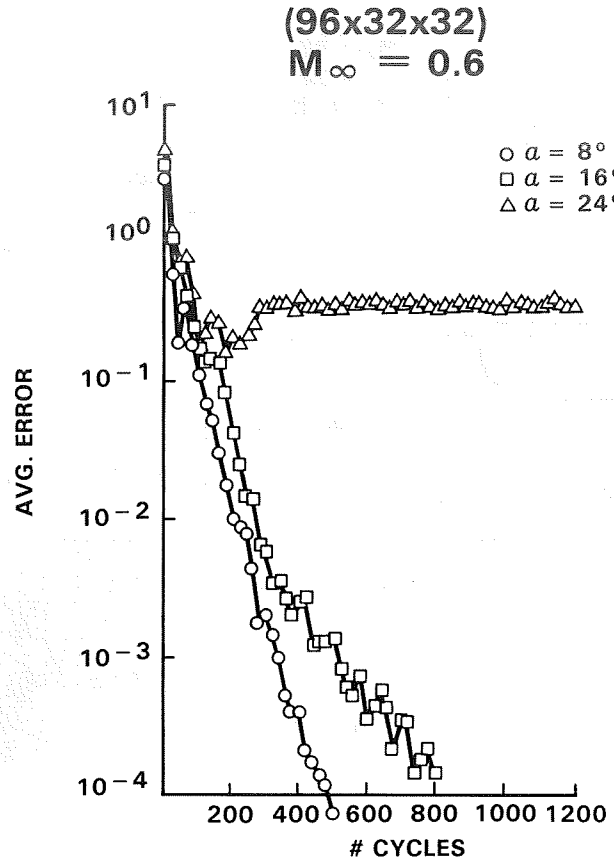

Figure 13. Convergence history for a fine grid (96 × 32 × 32) at three different angles of attack.

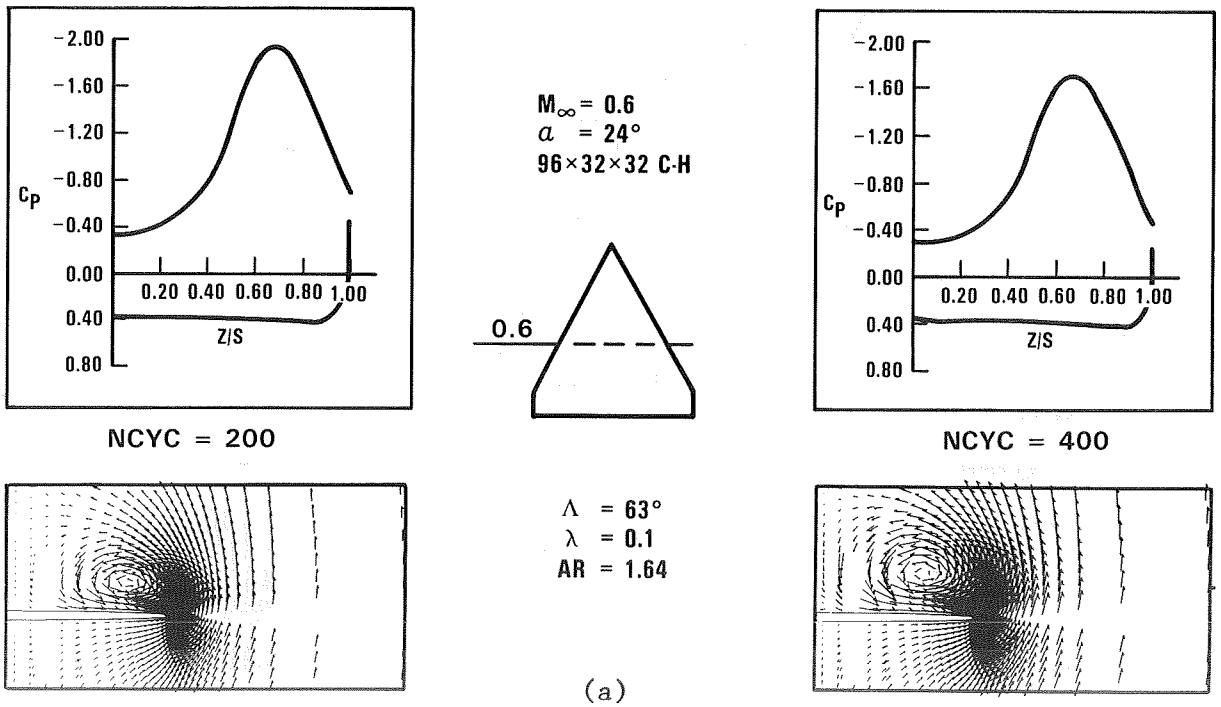

Figure 14. Spanwise pressure distributions and velocity vectors for six different times in integration process (x/c = .6).

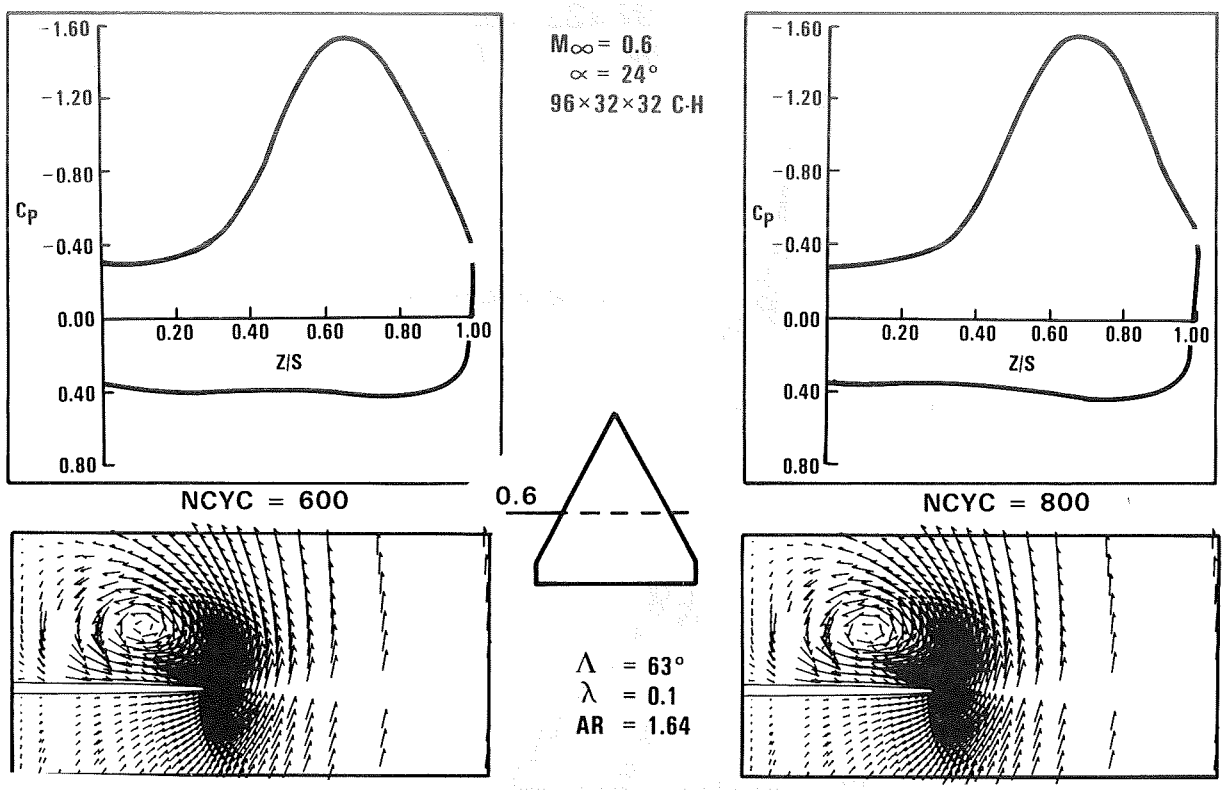

(b)

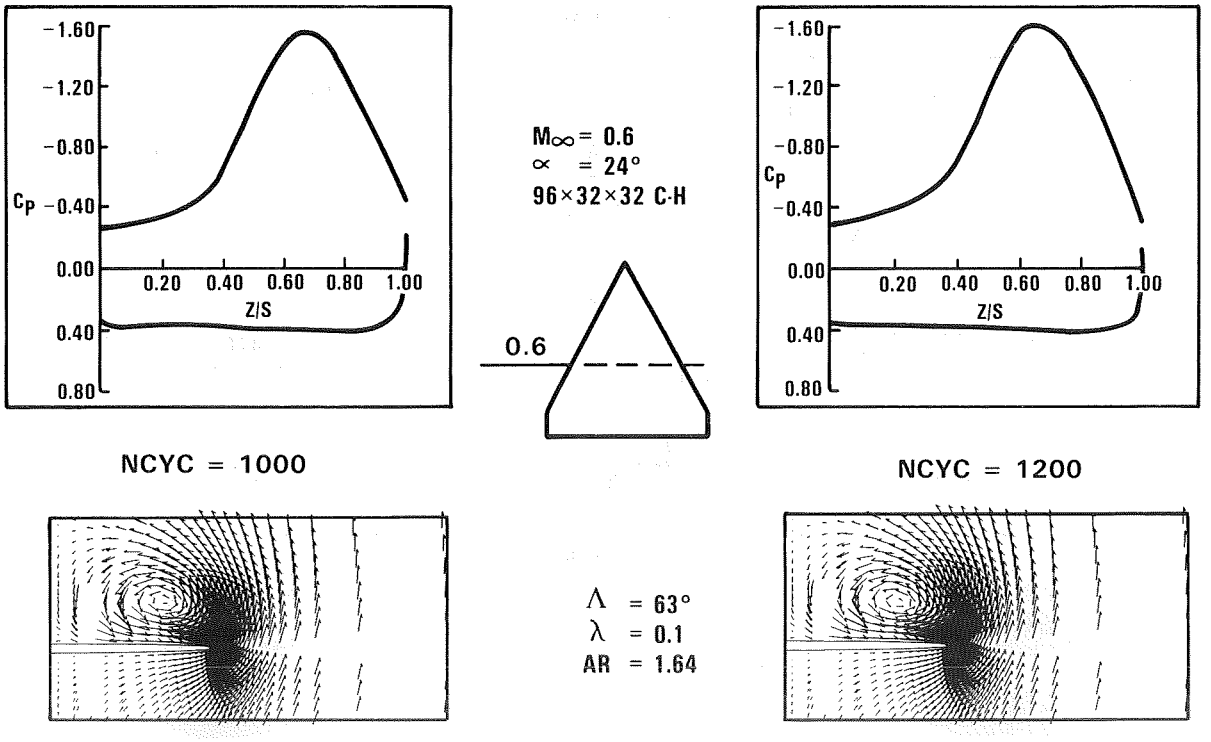

(c)

Figure 14. Concluded

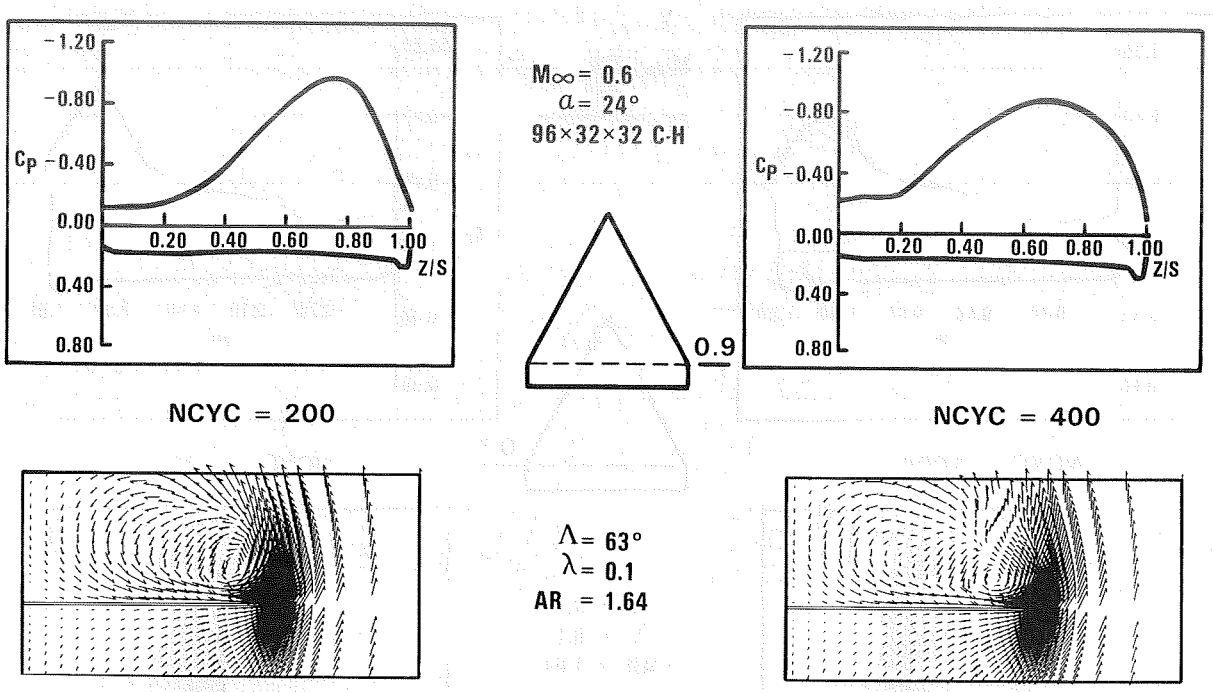

(a)

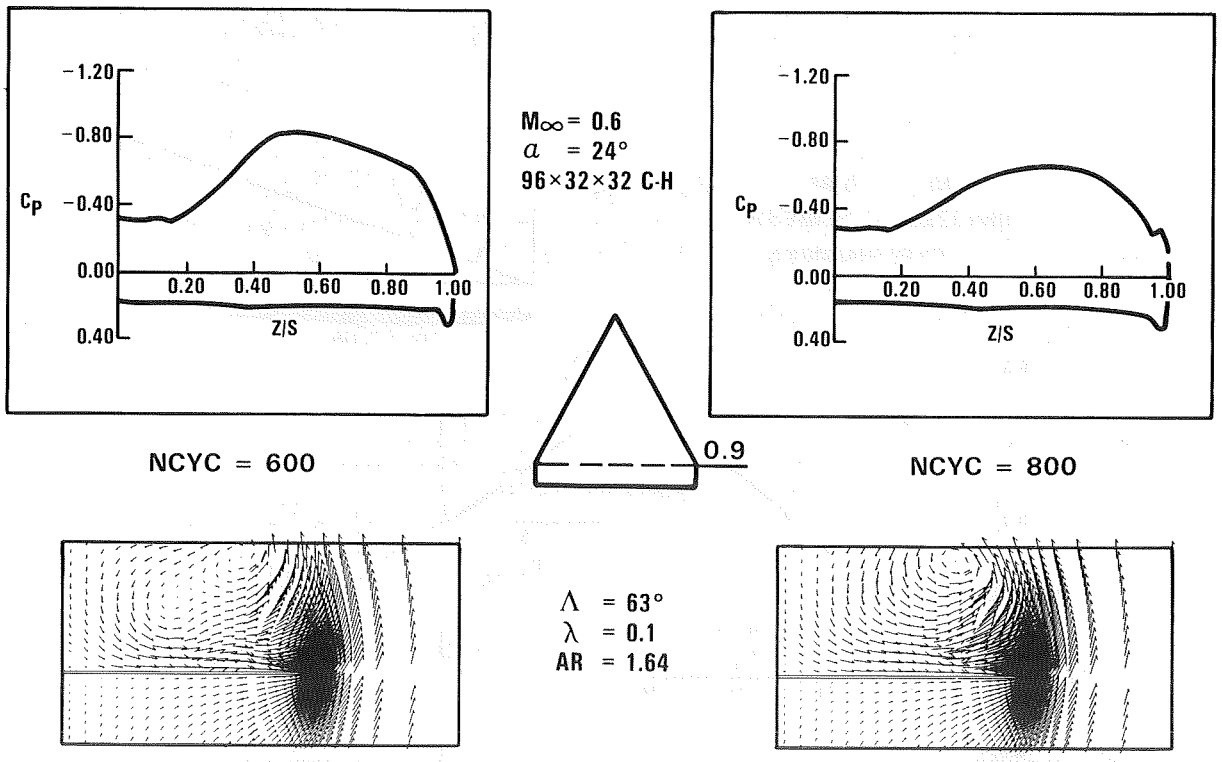

(b)

Figure 15. Spanwise pressure distributions and velocity vectors for six different times in integration process (x/c = .9).

C-4

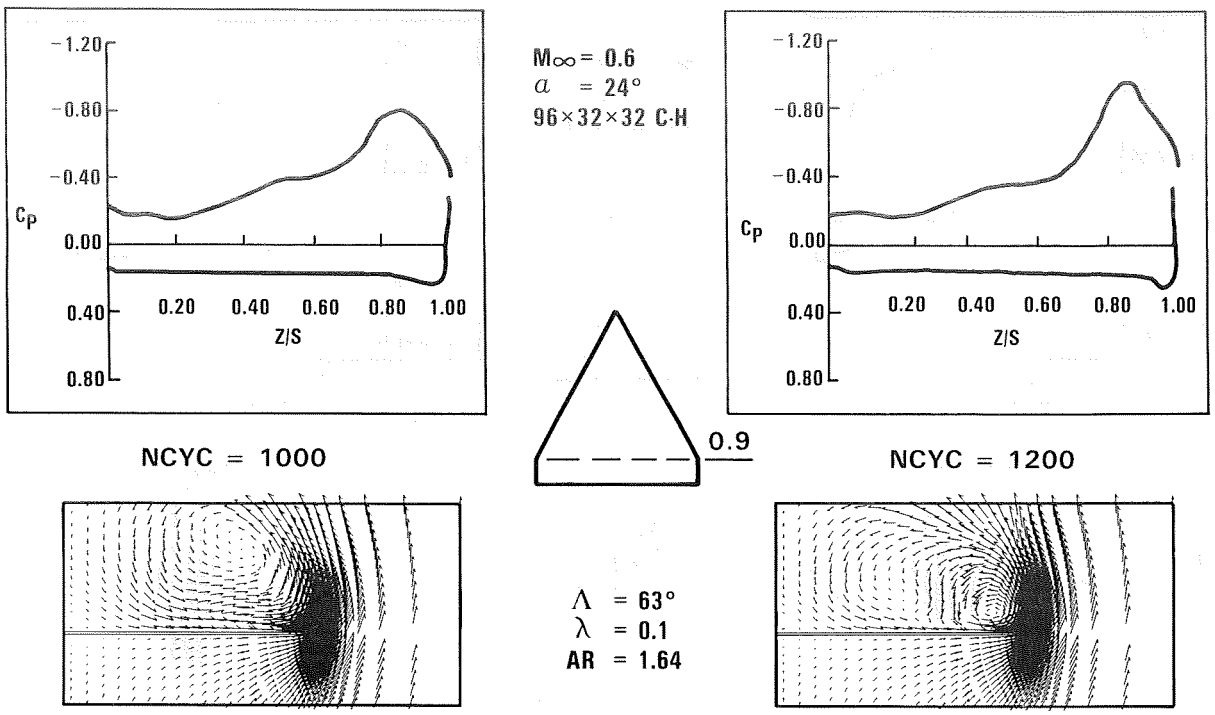

(c)

Figure 15. Concluded

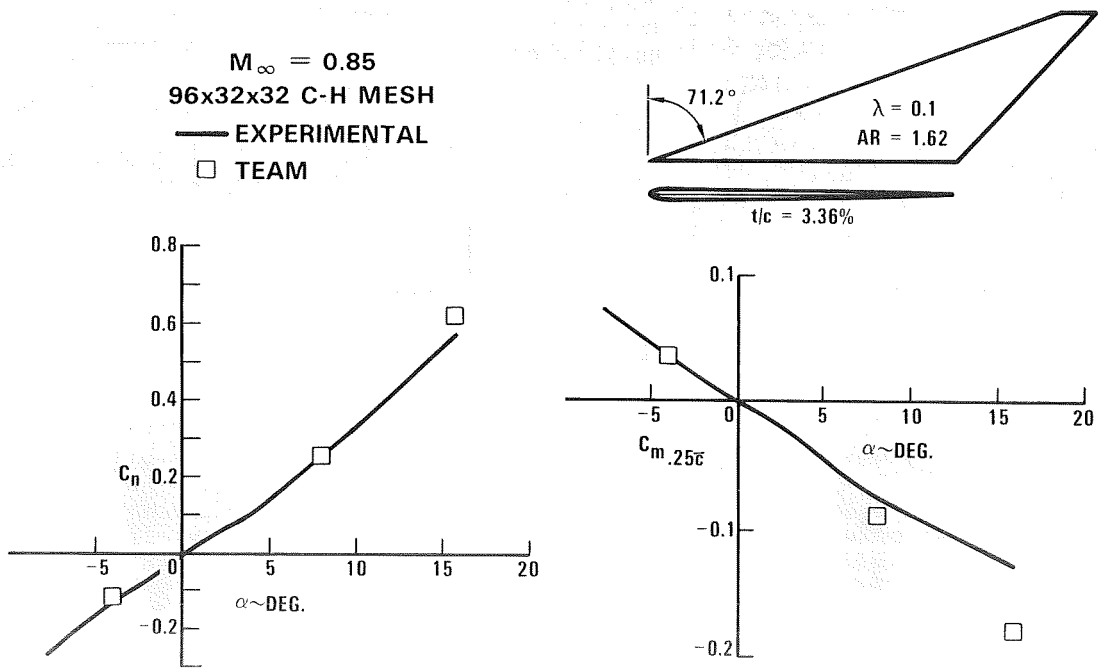

Figure 16. Computed and measured aerodynamic coefficients for an arrow wing.

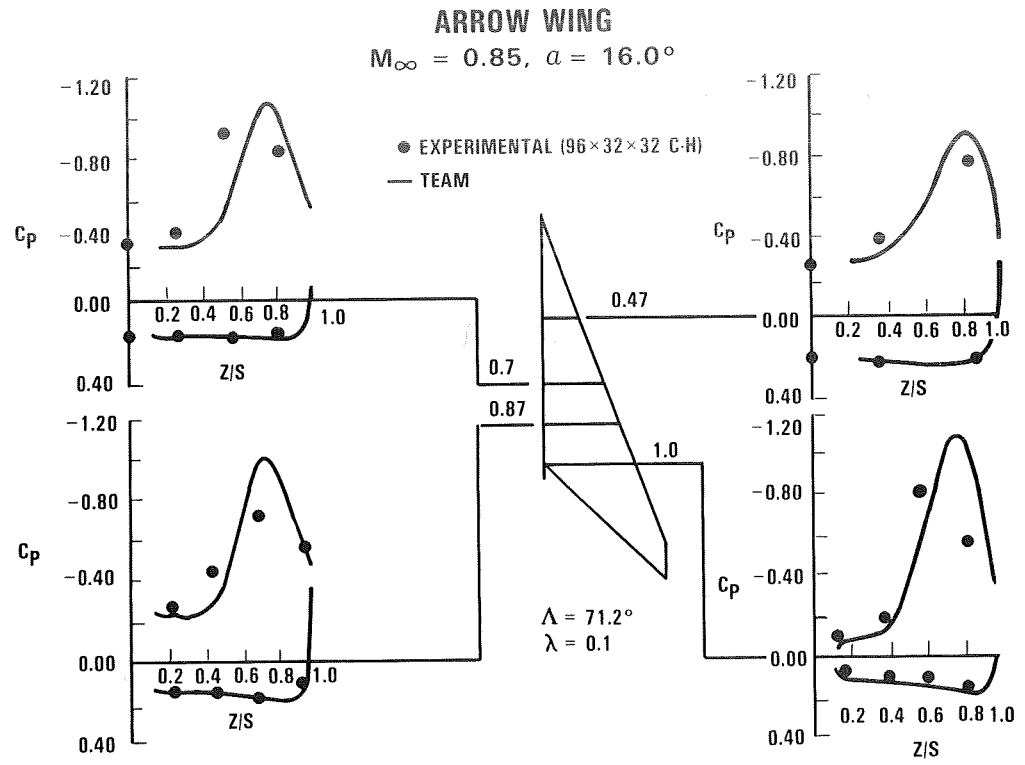

Figure 17. Computed and measured pressure distributions for four spanwise locations.

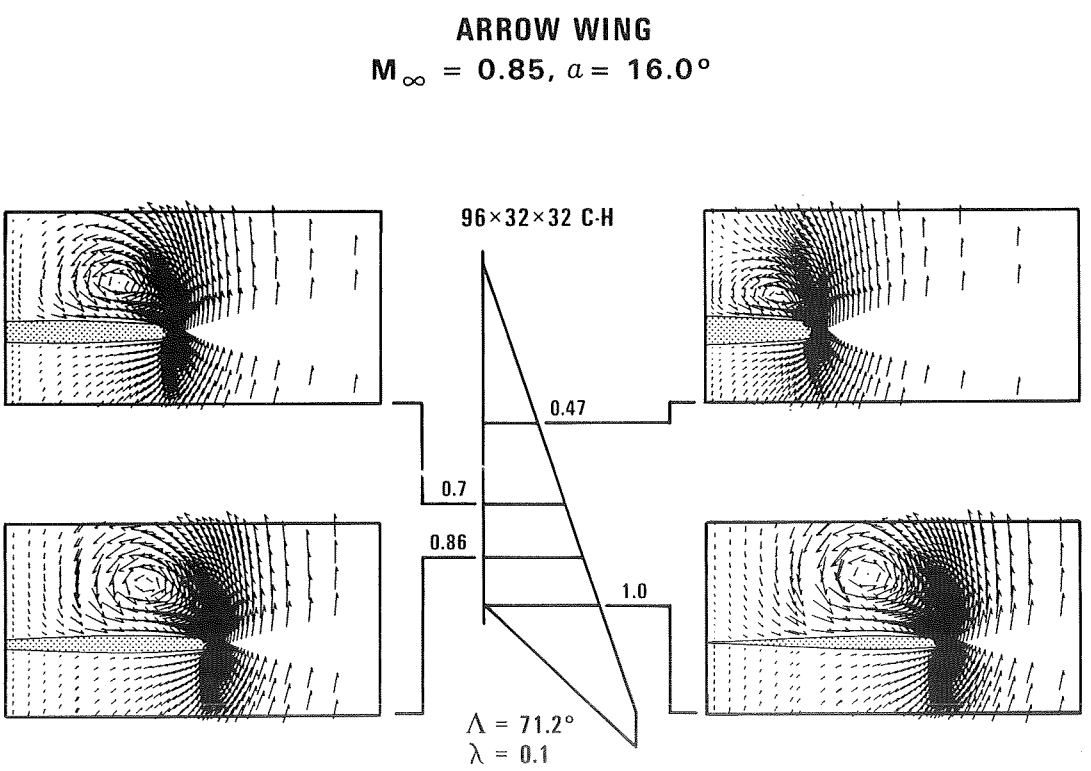

Figure 18. Computed velocity vectors for four spanwise locations.